Comprehensive mouse gut metagenome catalog reveals major difference to the human counterpart

Silas Kieser[1,2,3], Evgeny M. Zdobnov[3,4,5,*] and Mirko Trajkovski[1,2,5,*]

[1]Department of Cell Physiology and Metabolism, Faculty of Medicine, University of Geneva, Centre Medical Universitaire, Geneva, Switzerland.

[2]Diabetes Center, Faculty of Medicine, University of Geneva, Geneva, Switzerland.

[3]Swiss Institute of Bioinformatics, Geneva, Switzerland.

[4]Department of Genetic Medicine and Development, Faculty of Medicine, University of Geneva, Centre Medical Universitaire, Geneva, Switzerland.

[5]Institute of Genetics and Genomics in Geneva (iGE3), University of Geneva, Geneva, Switzerland.

*Correspondence: Mirko.Trajkovski@unige.ch; Evgeny.Zdobnov@unige.ch

Lead contact: Mirko.Trajkovski@unige.ch

Keywords: Mouse, Human, Microbiome, Metagenome

Abstract

Mouse is the most used model for studying the impact of microbiota on its host, but the repertoire of species from the mouse gut microbiome remains largely unknown. Here, we construct a Comprehensive Mouse Gut Metagenome (CMGM) catalog by assembling all currently available mouse gut metagenomes and combining them with published reference and metagenome-assembled genomes. The 50'011 genomes cluster into 1'699 species, of which 78.1% are uncultured, and we discovered 226 new genera, 7 new families, and 1 new order. Rarefaction analysis indicates comprehensive sampling of the species from the mouse gut. CMGM enables an unprecedented coverage of the mouse gut microbiome exceeding 90%. Comparing CMGM to the human gut microbiota shows an overlap 64% at the genus, but only 16% at the species level, demonstrating that human and mouse gut microbiota are largely distinct.

Introduction

Mouse is the most used model for studying the microbiota importance due to several factors: availability of samples from different parts of the gastrointestinal tract, treatment options, controlled housing environment and diet, defined genetic background, and ethical considerations. However, the mouse gut microbiota has been poorly characterized, and only a fraction of the diversity observed by 16S rDNA sequencing is represented by genomes in public databases (Lagkouvardos et al., 2016). The majority of mouse microbiome studies are performed by sequencing variable regions of the 16S, sometimes mislabeled as metagenomics. While this technique has allowed a general overview of the microbiota down to the genus level, it is not suited for identifying species for most organisms (Johnson et al., 2019). Different species from the same genus and even subspecies from the same species can exert distinct functions (Costea et al., 2017), stressing the importance of annotating the gene content at the lowest taxonomic level.

Shotgun metagenomics allows studying the full microbiota diversity of an environment, including uncultured microorganisms, viruses, and plasmids. However, its interpretation is limited by the availability of reference genomes. Previous efforts led to the creation of a gene catalog of the mouse metagenome (MGC v1) (Xiao et al., 2015), by sequencing fecal samples from mice with different genotypes and housed in different conditions. This catalog enables the functional annotation of genes and allows up to a 50% mapping rate of fecal shotgun sequences. However, the mapping rate of sequences from cecum samples is only 37%, and the catalog does not contain genomic references. Recently developed algorithms enable the assembly of genomes from metagenomes, leading to a recovery of new species from the human gut and other environments (Almeida et al., 2019; Nayfach et al., 2019; Parks et al., 2017; Pasolli et al.; Stewart et al., 2018). The integrated mouse gut metagenomic catalog (iMGMC) (Lesker et al., 2020) increased the fraction of reads mapped to genes compared to the MGC v1. However, mapping to the recovered metagenome-assembled genomes (MAGs)

remained about 40% (Lesker et al., 2020). Lesker *et al.* also generated a set of 13,619 mouse-specific MAGs (mMAG) not integrated into the iMGMC, which was made available for further studies.

Here we report the creation of the Comprehensive Mouse Gut Metagenome (CMGM) collection by assembling gut microbiomes sequenced by us and all publicly available mouse metagenomes. This resource improves the mapping rate of genomic reads from mouse fecal and cecum metagenomes to over 90.5%, provides full classification down to species level, and enables uncovering compelling functional insights linking them to the driver species. This nearly complete catalog of the mouse gut bacterial species allows comparison between the newly assembled mouse gut microbiomes and the human counterpart, highlighting major differences between human and mouse.

Results

Assembly of high-quality genomes from mouse gut metagenomes

We selected all metagenomic datasets associated with the mouse intestinal tract that are sequenced as paired-ends from the NCBI sequence read archive. To these, we added samples generated by our lab resulting in 1226 datasets (Table S1). Each sample was processed using metagenome-atlas (Kieser et al., 2020), which handles pre-processing, assembly, and binning of the metagenome datasets. We included all mouse-associated bacterial genomes retrieved from RefSeq belonging to 331 species (Table S2, Fig. S1), which also incorporates genomes from mouse specific culture collections: Oligo-mouse-microbiota (Garzetti et al., 2017) (12 genomes), and Mouse Gut Microbial Biobank (mGMB, 41 genomes) (Liu et al., 2020). As genomes of the mouse Intestinal Bacterial Collection (miBC, 53 genomes) (Lagkouvardos et al., 2016) were not available, we assembled them from the raw reads. To this extensive new set, we included all MAGs produced by Lesker *et al.*, thereby adding comprehensiveness to the newly assembled catalog (Fig. S1). All genomes were filtered based on fragmentation

(N50 >5000) and a quality score calculated from the output of checkM (Parks et al., 2015) as 'completeness minus 5 times contamination'. Bins with a quality score of <50 were excluded, resulting in a set of 49,'195 MAGs of which 15'355 (31%) had high quality (Quality score >90, Fig. S2A+B). Surprisingly, some reference genomes had contamination values of 100%, suggesting that the sequenced genomes consist of multiple strains. In total, 13 reference genomes did not pass the quality filtering, and we included 816 reference genomes in the CMGM collection, resulting in a total of 50'011 genomes.

While MAGs were more fragmented and had a lower median quality score than the reference genomes, the quality score and N50 of the high-quality MAGs were comparable to the values of the references (Fig. S2B). For 60% of the reference genomes, we recovered MAGs that align to them with high coverage and identity (average nucleotide identity (ANI) >95%, IQR 94-99%, Fig. S2C). This result validates our metagenome assembly approach to recover "reference quality" genomes *de novo*. Some of the remaining differences might be attributed to strain variation, as the coverage is higher for more similar genomes (Fig. S2C).

Since we assembled genomes from individual samples, the same strain could have been recovered multiple times, especially if different gut locations of the same mouse were sampled. To remove this potential redundancy, we clustered the genomes based on the ANI calculated using bindash (Zhao, 2018). 95% ANI was used as a threshold to delineate genomes from the same species (Jain et al., 2018; Olm et al., 2019). For each species cluster, the genome with the highest quality and lowest fragmentation was selected as representative, but reference genomes were preferred over MAGs. The species representatives were annotated using DRAM (Shaffer et al., 2020) to obtain the functional potential and the genomic taxonomy database (GTDB (Parks et al., 2018, 2020)). For unclassified species, we manually annotated the taxonomy based on the phylogenetic tree constructed using the GTDB marker genes. Species that contain a reference genome of an isolate were counted as cultured, even when they might not be available from official culture collections. Similarly, species named after an isolated strain in GTDB were annotated as cultured.

91 **CMGM species comprehensively cover the mouse gut metagenome**

92 The CMGM genome collection represents 1'699 species, and we discovered 226
93 new genera, 7 new families, and 1 new order (Fig. 1A). 78.1% of the CMGM species
94 are uncultured, with only 15% having a mouse-specific cultured strain. 164 species
95 do not have a cultured species even at the order level. The sum of cultured species
96 accounts on average for less than 25% of the mouse metagenome.

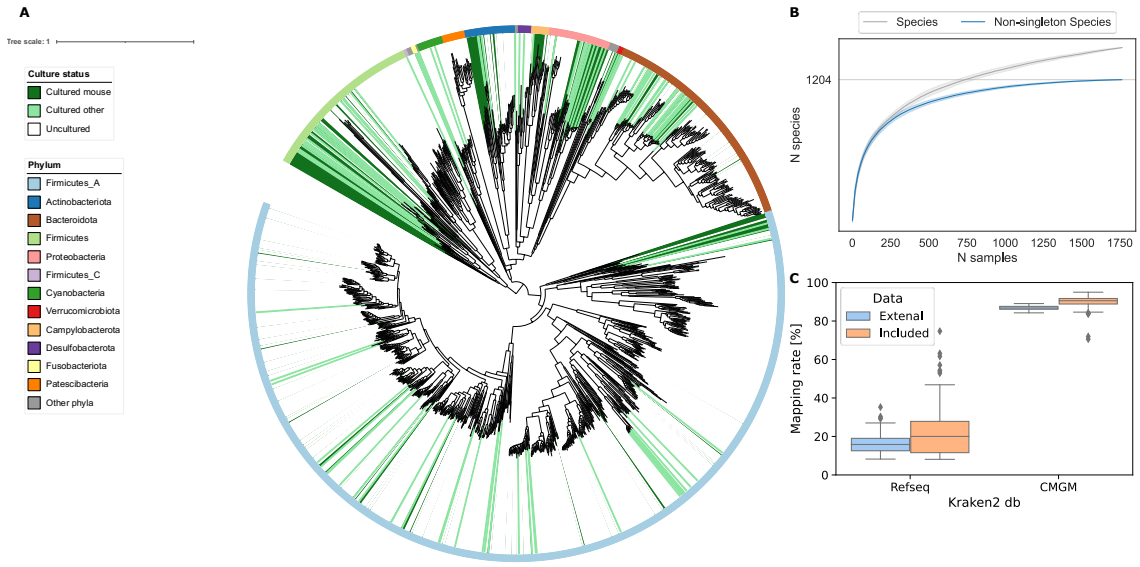

Fig. 1| CMGM comprehensively covers the mouse metagenome
A, Maximum-likelihood phylogenetic tree of the 1699 bacterial species detected in the mouse gut. Clades are colored by culture status, and the color ring indicates the phylum. **B,** Rarefaction curves of species. **C,** Comparison of mapping rates of the mouse gut metagenome.

97 Rarefaction analysis shows that the number of species reached a saturation point
98 at 1240 species when considering species with at least two conspecific genomes
99 (Fig. 1B). This indicates that the CMGM catalog contains all species commonly
100 living in the mouse gut. More rare species can still be discovered, as indicated by
101 the non-converging rarefaction curve with singletons (species that were
102 recovered in one only sample). CMGM achieves a mapping rate of the mouse
103 metagenome of 90.5% using Kraken2 (Wood et al., 2019), which is a 4.5-fold
104 increase compared to the standard Kraken database that contains all RefSeq
105 genomes from archaea, bacteria, viruses, and plasmids (Fig. 1C). To independently
106 evaluate the mapping rate of the CMGM catalog, we used an external dataset of

cecum samples, which was explicitly left out from this catalog. The CMGM species covered 87.7% of the metagenomic reads, which represents an over 5.5-fold increase to the RefSeq database (Fig. 1C).

CMGM enables comparative analysis of mouse metagenomes by relating functional changes to driver species

To illustrate how this catalog allows discovering compelling biological insights, we analyzed the metagenome from mice exposed to cold ambient air temperature. Cold exposure is a stimulus that activates the classical brown fat and promotes beige cell development within the subcutaneous white adipose tissue (Cannon and Nedergaard, 2017; Chechi et al., 2013; Stojanović et al., 2018). As such, it is an extensively used intervention for enhancing thermogenic and mitochondrial activity in adipose tissues, leading to decreased adipose tissue amount and improved glycemic status. We (Chevalier et al., 2015), and others (Ziętak et al., 2016) showed that cold exposure leads to a marked shift of the microbiota composition observed by 16S analysis, which is in itself sufficient to improve the insulin sensitivity, induce tolerance to cold, increase the energy expenditure and lower the fat content– an effect in part mediated by activation of the brown fat (Chevalier et al., 2015; Ziętak et al., 2016) and browning of the white fat depots in the cold microbiota-transplanted mice (Chevalier et al., 2015; Cypess et al., 2015; Ghorbani et al., 1997; Guerra et al., 1998; Kopecky et al., 1995). These results indicate an existence of a microbiota-fat signaling axis; however, the signaling cascades mediating this process remain poorly understood.

As noticed previously (Chevalier et al., 2015), here we confirmed that *Akkermansia muciniphila*, the only representative of the phylum *Verrucomicrobiota* was eliminated by cold exposure (Fig. 3A). We found that cold exposure leads to a decrease of the family *Muribaculaceae* and an increase of *Lachnospiraceae* and *Oscillospiraceae.* The species NM07-P-09 sp004793665 (the only species from the phylum *Actinobacteriota*) and three other *Muribaculaceae* species were equally significantly decreased (Fig 3A, $P_{BH} < 1e-4$). The phylum *Proteobacteriota*,

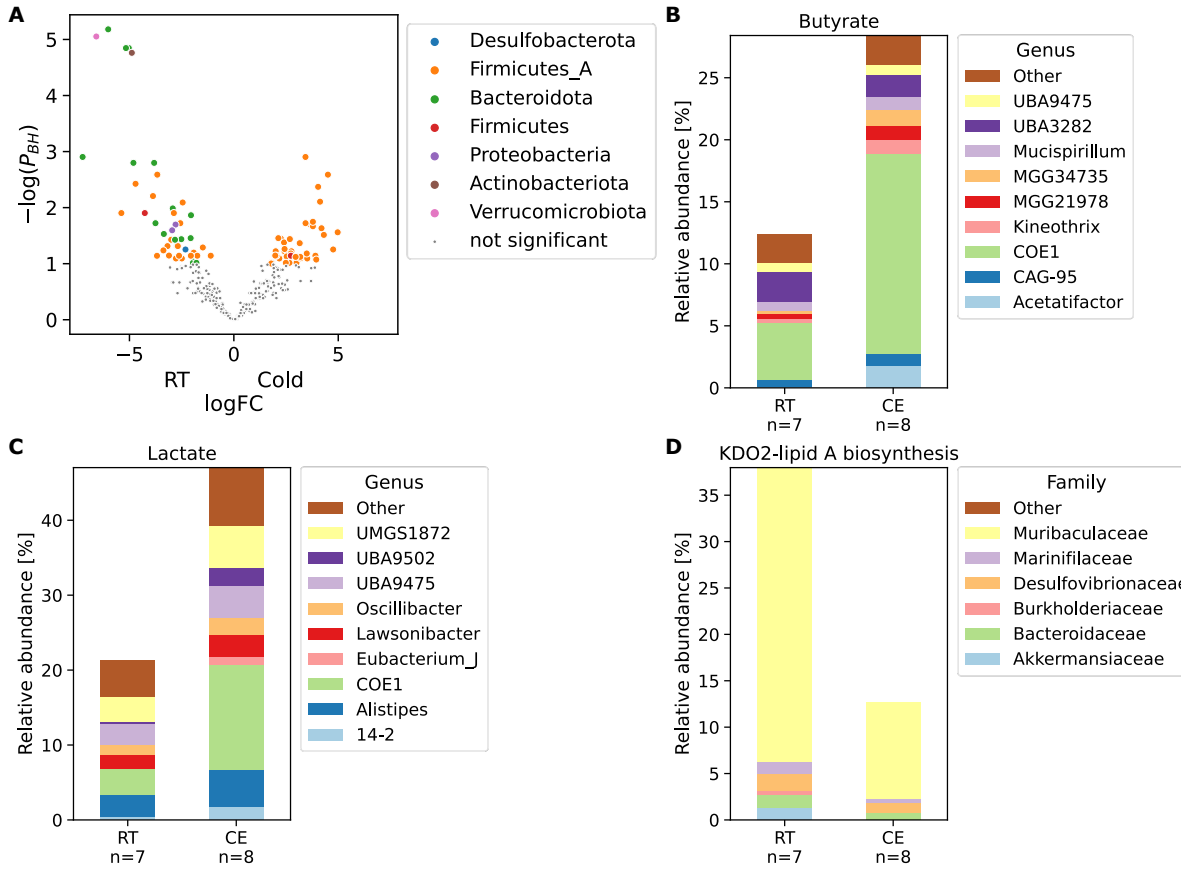

Fig. 2| CMGM links functional changes to driver species

A, Volcano plot of species changes in mouse cecal microbiota upon cold exposure. Significantly changed species are colored by their phylum. P_{BH}: P-value corrected for multiple testing using Benjamini-Hochberg **procedure. B-D,** Bar plots of significantly changed pathways in mouse cecal microbiota upon cold exposure. The contribution to the relative abundance of each module is partitioned by genus B+C and family D.

CE: Cold exposure, RT: Room temperature control

consisting of two species, was significantly decreased. On a functional level, cold exposure led to a doubling of butyrate and lactate production. These changes were mainly due to the increase of the family *Lachnospiraceae,* specifically the increase of the uncultured genus *COE1* (Fig. 3B, C). To address whether these uncovered metagenomic changes are indeed reflected in differences of the actual metabolite levels, we looked at the germ-free mice transplanted with microbiota from the cold-exposed mice or from their RT-kept controls. Transplantation of the cold-adapted microbiota led to an increase in the production of butyrate,

144 lactate, propionate, and succinate in the recipients' cecum compared to germ-
145 free mice inoculated with microbiota from control mice (Fig. S3). Interestingly,
146 the increased lactate was also measured in the cecum and serum of mice with an
147 intermittent fasting feeding regime (Li et al., 2017), which has been shown to
148 induce browning via the induction of the Vascular endothelial growth factor (Kim
149 et al., 2017). Similarly, succinate is linked to the increase of thermogenesis (Mills
150 et al., 2018). We found a decrease of the prokaryotic succinate dehydrogenase,
151 which metabolizes succinate to fumarate, suggesting a mechanistic link between
152 the cold-induced microbiota changes and the adipose tissue browning.

153 We also observed a decrease in Lipopolysaccharide (LPS) synthesis, both in an
154 LpxL-LpxM–dependent and –independent way, primarily attributed to the cold-
155 induced reduction of *Muribaculaceae* (Fig. 3D). LPS administration leads to
156 reduced core body temperature and heat release, correlated with mitochondrial
157 dysfunction (Okla et al., 2015). In contrast, genetic deletion of the LPS receptor,
158 the toll-like receptor 4 (TLR4), leads to resistance against high caloric diet-
159 induced obesity, improved glucose tolerance and insulin sensitivity, and adipose
160 tissue browning (Fabbiano et al., 2018). These findings suggest an additional
161 possible link between the cold-induced microbiota changes and adipose tissues
162 both at mechanistic and bacterial level, contributing to improved insulin
163 sensitivity and browning of the white fat

164 This example illustrates the CMGM catalog's usability as a reference for
165 metagenomic studies, enabling discovering precise and comprehensive changes
166 of species and the related function induced by a treatment or a disease. The
167 CMGM sets the ground for reanalysis of the existing datasets for uncovering
168 species and bacterial functions that are involved or altered by the condition of
169 interest.

170 **Comparison between human and mouse gut microbiomes**

171 Studying mouse microbiota and its impact on the host as a proxy for humans
172 implies their similarities. However, 16S rDNA profiling and gene catalogs do not
173 allow a comprehensive analysis of the analogy between human and mouse
174 microbiota down to species level. Also, much fewer species from the mouse gut

175 are sequenced than from the human gut (Hugenholtz and de Vos, 2018). The
176 CMGM catalog, together with the recent creation of genome collections from the
177 human gut (Almeida et al., 2021), renders this comparison possible. Here, we
178 compared the species from CMGM to the ones from the unified human
179 gastrointestinal genomes (UHGG) (Almeida et al., 2021) and applied the same
180 criteria as for clustering (ANI > 95%). We annotated all species from both hosts
181 with the genome taxonomy database (GTDB, release 5) and curated the
182 unannotated taxonomic levels to allow a consistent taxonomic comparison from
183 domain down to species level.

184 More than half of the species in both microbiomes belong to the phyla
185 *Firmicutes_A* (Fig. 3A). *Firmicutes_A* and *Bacteroidota* (*Bacteroidetes*) are the
186 most abundant phyla in both human and mouse microbiomes. Overall, 16 phyla
187 have representatives in both human and mouse microbiome, and 5 are only found
188 in human and not in mice. In contrast, the phyla *Deferribacterota, Thermotogota,*
189 and the two species *Chlamydia muridarum* and *Chlamydophila psittaci,* which
190 represent an own phylum, are specific to mice. No archaea were reconstructed
191 from the mouse gut metagenome, whereas 0.4 % of the genomes in the human
192 gut from the UHGG belong to this domain. At the family level, humans and mice
193 share 98 of the 122 taxa (80% overlap, Fig. 3B), whose average abundance in
194 human and mouse microbiota are correlated (r=0.55, p=1.1e-09). The families
195 *Lachnospiraceae*, *Oscillospiraceae*, and *Butyricicoccaceae*, have high abundance
196 in both human and mice. The family *Muribaculaceae* is 5.6 times more abundant
197 in mice than in humans, whereas *Bacteroidaceae* is 4 times less. While at the
198 genus level, 282 of 440 of taxa are shared (64% overlap, Fig. 3B) in line with results
199 based on 16S rDNA sequencing (Krych et al., 2013, the abundance of the genera
200 showed only a weak correlation (Fig. 3C, r=0.20, p=5e-05). Intriguingly, the genus
201 *Collinsella* (phylum *Actinobacteria*), associated with atherosclerosis and
202 rheumatoid arthritis (Chen et al., 2016; Karlsson et al., 2012), is represented with
203 579 species in the human but not found in the mouse metagenome.

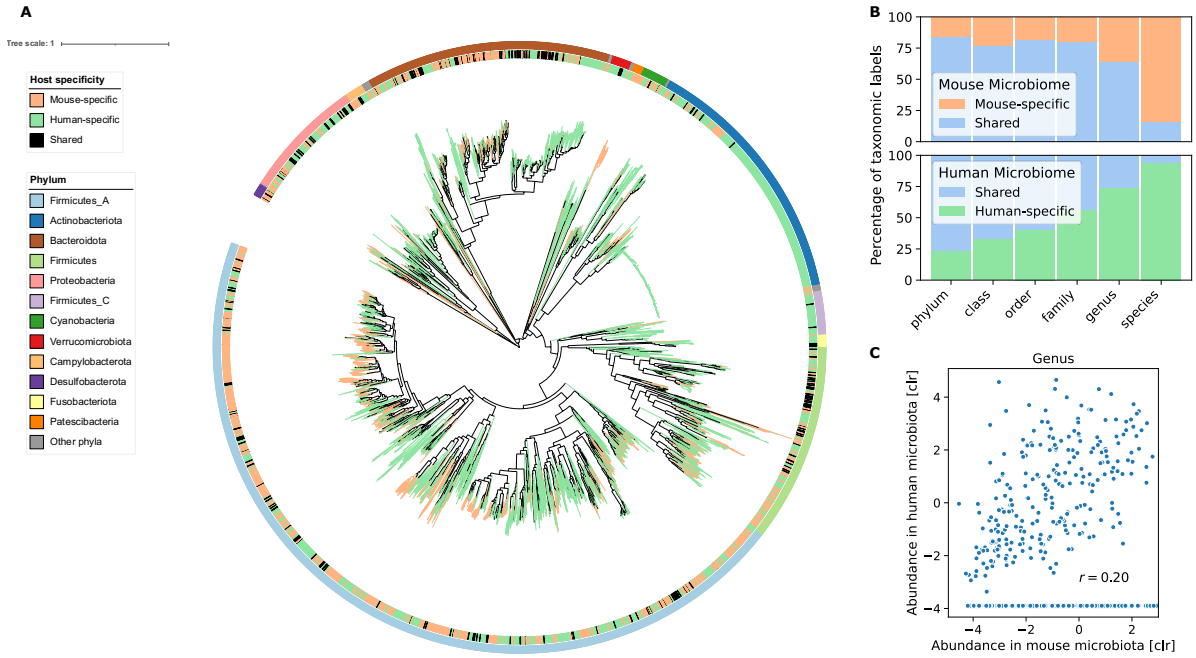

Fig. 3| Human and mouse guts harbor distinct bacterial species.
A, Maximum-likelihood phylogenetic tree of the bacterial species from UHGG and CMGM. The innermost color ring and the tree branches are colored by host specificity. The outermost color ring indicates the phylum attribution. **B,** Percentage of shared and host-specific taxa from CMGM and UHGG at different taxonomic levels. **C,** Correlation of average abundance of genera in human and mice microbiotas. Genera that are not detected in human but present in mouse have an imputed value of -4. CLR = centered log ratio.

Strikingly, from the 1699 CMGM species, only 271 (16%) were identified in the human gut microbiota (Fig. 3A, B). The shared species account, on average, for 14.4% of the mouse gut microbiome, and 36 of the 1'699 species in CMGM belong to mouse-specific families. This shows major differences between human and mouse microbiota at species level, demonstrating that mice and human microbiota are largely distinct. These findings effectively challenge our view on the analogy between human and mouse microbiota and may impact the experimental designs, analyses and approaches for studying the human gut microbiome using mouse as a proxy for human.

Discussion

We generated a comprehensive catalog of the mouse gut metagenome: 50'011 genomes from 1'699 species. This resource enables the mapping of over 90% of the mouse metagenome. Three-quarters of the species are uncultured. Some do not even have a representative at the order level, pointing to the CMGM catalog as a basis for targeted culturing of these missing strains.

Saturation in the rarefaction analysis shows that the CMGM catalog contains all species commonly living in the mouse gut. Nevertheless, we cannot exclude that new samples may add diversity that is not part of the CMGM, for example, species present in single samples or wild mice. However, CMGM is built by assembling all publicly available data from the most used mouse strains, thus comprehensively representing the microbiome of laboratory mice. Comparing the mouse microbiota to the human counterpart reveals overlap and correlation of the average abundance from phylum down to family level. As suggested by amplicon sequencing (Krych et al., 2013), the genera are qualitatively the same but quantitatively different. We observed only a medium correlation between their average abundances in human and mouse microbiota. Whereas a comprehensive and precise comparison at species level between the two microbiomes was not previously feasible (Hugenholtz and de Vos, 2018; Johnson et al., 2019), the comparison of CMGM with the UHGG collection reveals an overlap of only 16% of the species.

While the overlap at the genus and higher taxonomic levels may imply a functional similarity of the human and mouse microbiome, this assumes that functions are conserved within a taxon. While for some functions this is indeed the case, the functional annotation is precisely biased towards conserved functional annotations, which can be transferred from model organisms to less-studied bacterial species. Species from the same genus, even strains from the same species, can have contrasting functions. Strains from the same species can differ in up to 30% in their gene content (Van Rossum et al., 2020) that may help strains from the same species to adapt to different environments. This is especially well studied for the species *Limosilactobacillus reuteri,* which has mouse- and human-

adapted strains, however with very different functions (Dheilly et al., 2020; Frese et al., 2011). The different abundance of the mouse and the human microbiome at the genus level, indicted by the weak correlation of average abundance (r = 0.2), compromises even the transferability of the conserved functions at genus level.

Different ways can be envisaged to overcome these challenges. For example, creating 'humanized' mouse models by advanced transplantation of human gut microbiota into germ-free mice, or complementing the work by exploring additional animal models (Nguyen et al., 2015). To leverage data produced using conventional mice, it will be important to uncover functional homologs between the species adapted to mouse and human microbiota, e.g., by identifying 'guilds' (Root, 1967), groups of species that use the same type of resources in a similar way. The provided consistently functionally annotated species of the human and mouse microbiome lay the basis for such work.

The mouse studies included in the CMGM contain biological insights that were not accessible previously, for example, because they relate to previously unknown species, and incomplete genomes. The knowledge of the genomes and a nearly complete mapping rate is a basis for precise analysis on functional level. This enables uncovering species and bacterial functions that are involved or altered by the condition or treatment of interest. Our resource containing comprehensive collection of the species from the mouse gut and their functional capacity, sets the ground for reanalysis of the existing datasets, and allows analysis of the mouse gut microbiome at an unprecedented depth.

Author contributions

S.K. wrote the code, analyzed, and interpreted the data, and generated the figures. E.Z. and M.T. guided the project, interpreted the data, and supervised the work. All authors conceptualized the study and wrote the paper.

Acknowledgments

We are grateful to Christopher Rands for the critical reading of the manuscript and to all members from our labs for discussions. This project has received funding from the European Research Council (ERC) under the European Union's Horizon 2020 research and innovation programme (ERC Consolidator Grant agreement No. 815962, Healthybiota) to M.T.

Supplementary Figures

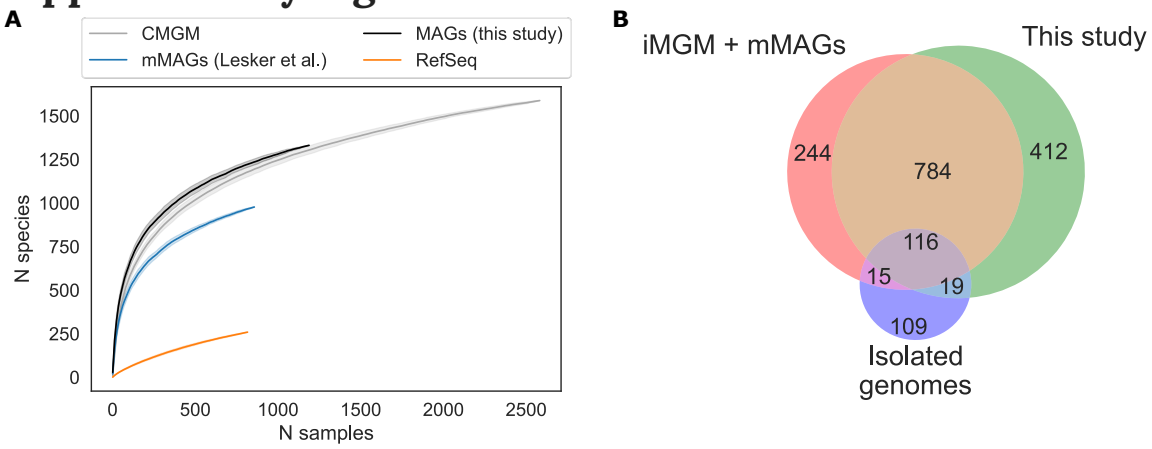

Fig. S1| Metagenome assembled genomes radically increase number of species from the mouse gut

A, Rarefaction curve of number of species recovered per sample from different sources and CMGM as a whole. **B.** Venn diagram of the species present in the different subsets of CMGM.

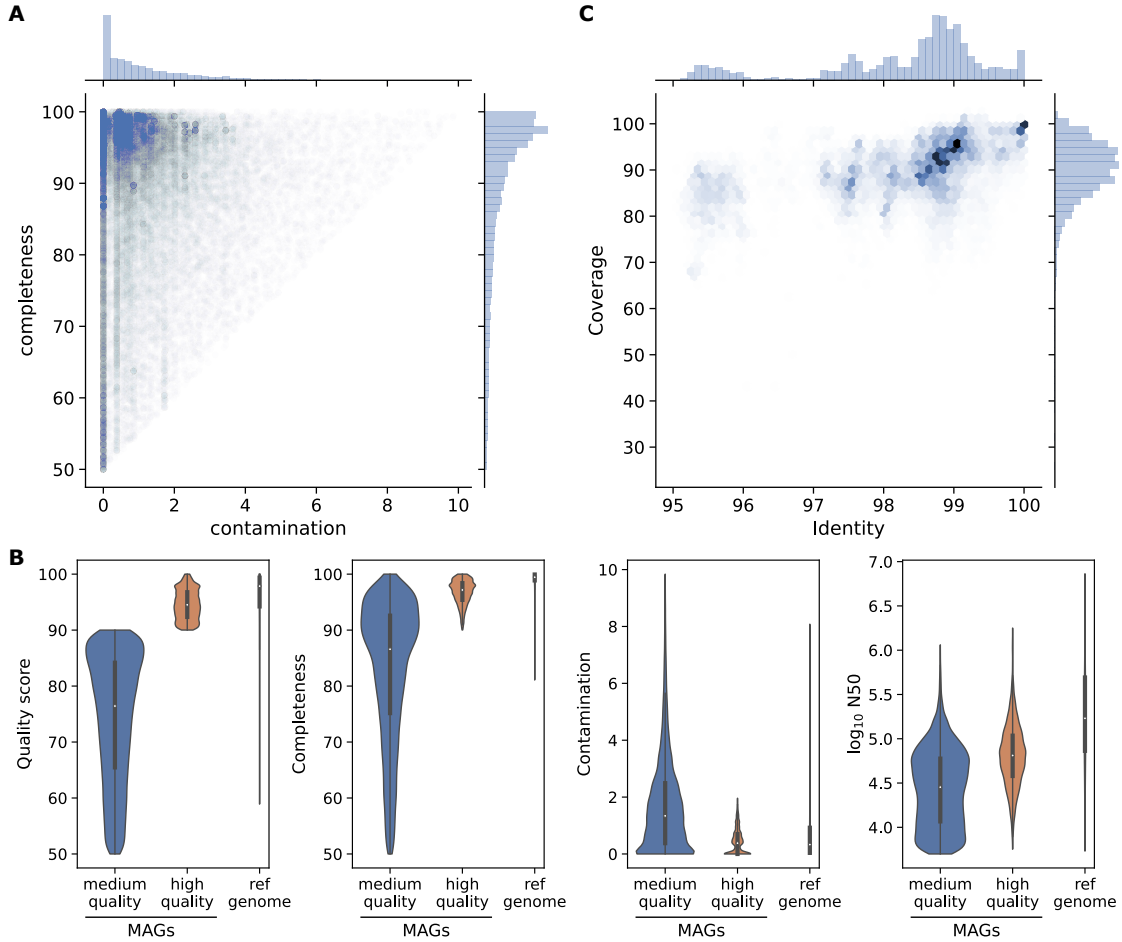

Fig. S2| Many metagenome-assembled genomes have comparable quality to reference genomes

A, Distribution of the MAGs included in the CMGM collection according to their completeness and contamination estimated with checkM. MAGs with ‘completeness -5×contamination`< 50 were excluded. **B,** Violin plots showing the quality score, completeness, contamination estimated using checkM and the $\log_{10}$ N50 from the assembly for the reference genomes and MAGs present in CMGM. **C,** Density plot of the coverage vs. identity of the MAGs alignments to 494 reference genomes

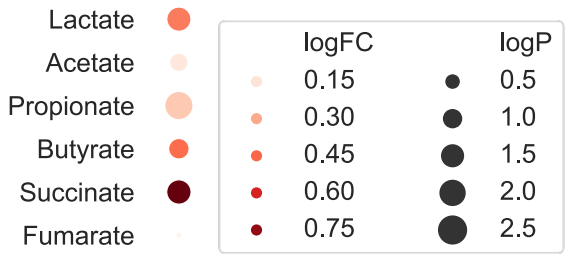

Fig. S3| Metabolite changes by cold adapted microbiome
Dot-plot of metabolite changes in ceca of germ-free mice transplanted with cold-adapted microbiota compared to RT-microbiota transplanted controls.

Supplementary Data

Available from https://ezmeta.unige.ch/CMGM/v1/SuppTables

Table S1 | Metagenome samples used to construct CMGM.
The table shows the metagenome samples used for the generation of CMGM. The CMGM_Id corresponds to the SRA read id, except for the samples sequenced by our lab. The table contains information retrieved from NCBI that was available for most of the samples: Name, description, Link to bioproject, collection data, country, and submission center. The column 'Source' specifies the organ from which the sample was taken. If the information was available in any of the metadata. Samples of the cold-adapted microbiota under the bioproject accession PRJNA646351 were sequenced for this study.

Table S2 | Reference genomes associated with the mouse gut.
The table shows the assembly information of reference genomes associated with the mouse gut. These genomes were filtered for completeness and contamination before integration into CMGM. The columns `Isolated` and `Cultured` label if the genome is Isolated and cultured. The `collection` describes if the genome is part of a mouse-specific culture collection. The genomes of the miBC collection are assembled for this study.

Methods

Sequencing of metagenomic data of mice

The sample collection and metagenomic sequencing were approved by the Swiss federal and Geneva cantonal authorities for animal experimentation (Office Vétérinaire Fédéral and Commission Cantonale pour les Expériences sur les animaux de Genève). Animals were on C57Bl/6J background, commercially available through Charles River, France. The mice experiment is detailed in (Chevalier et al., 2015). Paired-end metagenomic libraries were prepared from 100 ng DNA using TruSeq Nano DNA Library Prep Kit (Illumina) and size selected at about 350 bp. The pooled indexed library was sequenced in a HiSeq4000 instrument at the iGE3 facility (University of Geneva).

Collection of public metagenome and genomic data

We searched the sequence read archive (SRA, accessed December 2019) of the National Center for Biotechnology Information (NCBI) for all publicly available paired-end metagenome runs from the mouse microbiome. We specifically excluded samples from human origin and amplicon sequences and different body parts than the gut. We extracted 1226 metagenome runs belonging to 45 projects. Metadata was retrieved using BioServices (Cokelaer et al., 2013) and curated (Table S1). We retrieved 776 assemblies from RefSeq who were linked to a biosample collected from mouse (Table S2). We excluded reference genomes collected from other body parts than the gut or feces.

Metagenome assembly and binning

Metagenomics and genomic reads were processed using the metagenome-atlas v2.3 (Kieser et al., 2020) pipeline with the command ‘atlas run genomes’. In short, using tools from the BBmap suite v37.78, reads were quality trimmed, and contaminations from the mouse genome were filtered out. Reads were error corrected and merged before they were assembled with metaSpades v3.13 (Nurk et al., 2017). Contigs were binned using metabat2 v 2.14 (Kang et al., 2019) and

maxbin2 v2.2 (Wu et al., 2016), and their predictions were combined using DAS Tool v 1.1.1 (Sieber et al., 2018). For the assembly of the 53 genomes of the mouse intestinal bacterial collection, we used the assembly workflow of metagenome-atlas and set 'spades_preset: normal' which uses the basic spades as assembler. The quality of the genomes was estimated using checkM v1.1 (Parks et al., 2015).

Genome filtering and species clustering

Genomes with good enough quality were grouped into species with average nucleotide identity (ANI) > 95%. First, genomes with an estimated quality of 'completeness-5*contamination' < 50 or N50 <= 5000 were excluded. Then, all pair-wise average nucleotide identities (ANI) above 0.8 were calculated using bindash (Zhao, 2018). The genomes were pre-clustered into clusters that contain at least one pair of genomes above the threshold. Then each cluster was grouped into species by hierarchical clustering with average linkage using scipy (Virtanen et al., 2020). For each species cluster, the genome with the highest score based on the following formula was selected as the representative.

$$\text{Score} = \text{Completeness} - 5 \times \text{Contamination} + 0.5 \times \log(\text{N50}) + 100 \times \text{isIsolate}$$

Where Completeness and Contamination are estimated using checkM v1.1 (Parks et al., 2015), N50 is the N50 score of the assembly contiguity, and 'isIsolate' is 1 for isolates and 0 for MAGs, to ensure that isolated genomes are preferred over MAGs even if they have lower quality.

Phylogenetic and taxonomic analysis

The species representatives of both the CMGM and the unified human gastrointestinal genomes (UHGG) (Almeida et al., 2021) were annotated using the genomic taxonomy database toolkit (GTDB-tk v1.2 (Parks et al., 2018)) and the GTDB release 5. A maximum-likelihood tree for the CMGM alone and the CMGM combined with the UHGG based on the 120 bacterial marker genes from the GTDB was built using fasttree v2.1 (Price et al., 2010) and rooted at the midpoint. The phylogenetic trees are visualized with iTOL v5 (Letunic and Bork, 2019).

356 Unannotated, taxa from both human and mouse were manually annotated. New
357 orders, families and genera were defined at the relative evolutionary divergence
358 of close related annotated taxa.

359 **Inferring cultured status**

360 Species that contain a reference genome included in the CMGM catalog are
361 counted as cultured from a mouse origin. If GTDB-tk (Parks et al., 2018) was able
362 to annotate the species to a reference with ANI >95%, we counted the species as
363 cultured from a non-murine source. In both cases, if the reference genome was
364 excluded from RefSeq (i.e., metagenome-assembled genomes) or labeled as
365 uncultured we counted the species as isolated but not cultured.

366 **Quantification**

367 We build Kraken 2 and bracken (Wood et al., 2019) databases for the CMGM and
368 the UHGG based on our curated taxonomy. The mapping rates were calculated
369 as a fraction of the reads attributed with bracken at the species level to the total
370 reads. For comparison, we quantified reads using the standard Kraken2 database
371 accessible from https://benlangmead.github.io/aws-indexes/k2 (stand
372 December 2020). For most quantification, the mapped reads per genome were
373 summed, and the centered log-ratio (CLR) was calculated using the sci-kit bio
374 package (http://scikit-bio.org/) after imputing zeros using a multiplicative
375 replacement approach. To calculate the average species abundance in the
376 mouse and human metagenome, we used 184 fecal samples from the MGC v1
377 (Xiao et al., 2015) and a random subset of 1000 samples of the human
378 metagenome that is commonly used for benchmarking (Almeida et al., 2019). The
379 Pearson correlation between the abundance of taxonomic groups in the human
380 and mouse microbiota was performed with scipy v1.4.1 (Virtanen et al., 2020).
381 When relative abundance was used as a measure, we used BBsplit
382 (https://jgi.doe.gov/data-and-tools/bbtools/bb-tools-user-guide/) with the
383 parameters' ambiguous2=best minid=0.9' to map metagenomic reads to the
384 references with 90 identity. We estimated the genome coverage as the median
385 of coverage over 1000bp blocks.

386 **Functional annotation**

387 The species representatives of both the CMGM and the UHGG were annotated
388 using DRAM (Shaffer et al., 2020). A Kegg-module is inferred to be present if ¾ of
389 all the steps were present in a genome. As there are no modules for short chain
390 fatty acids in Kegg we created custom modules (see the 'Code' section). The
391 step-coverage was calculated with DRAM for all Kegg-modules. The
392 metagenome-side abundance of functional modules was calculated as the sum
393 of the relative abundances of all genomes containing a module. We used the
394 Welch test and Benjamini-Hochberg correction to estimate the significance of
395 changes in module abundance between experimental groups.

396 # Data Availability

397 The metagenomic samples sequenced for this study are available from the NCBI
398 sequence read archive under the project id PRJNA646351. The genomes
399 assembled in this study will be deposited under study accession PRJNA646353 and
400 are accessible now from https://ezmeta.unige.ch/CMGM/v1. The taxonomy,
401 functional annotation, and Kraken databases for both human and mouse are
402 available from the same link.

403 # Code Availability

404 The code for the analysis of the cold-exposed microbiota is available from
405 https://github.com/SilasK/CMGM

406 # References

407 Almeida, A., Mitchell, A.L., Boland, M., Forster, S.C., Gloor, G.B., Tarkowska, A., Lawley, T.D., and Finn,
408 R.D. (2019). A new genomic blueprint of the human gut microbiota. Nature *568*, 499–504.

409 Almeida, A., Nayfach, S., Boland, M., Strozzi, F., Beracochea, M., Shi, Z.J., Pollard, K.S., Sakharova, E.,
410 Parks, D.H., Hugenholtz, P., et al. (2021). A unified catalog of 204,938 reference genomes from the
411 human gut microbiome. Nat. Biotechnol. *39*, 105–114.

412 Cannon, B., and Nedergaard, J. (2017). Cell Metabolism Previews What Ignites UCP1? Cell Metab. *26*,
413 697–698.

414 Chechi, K., Carpentier, A.C., and Richard, D. (2013). Understanding the brown adipocyte as a
415 contributor to energy homeostasis. Trends Endocrinol. Metab. *24*, 408–420.

416 Chen, J., Wright, K., Davis, J.M., Jeraldo, P., Marietta, E. V., Murray, J., Nelson, H., Matteson, E.L., and
417 Taneja, V. (2016). An expansion of rare lineage intestinal microbes characterizes rheumatoid arthritis.
418 Genome Med. *8*, 43.

419 Chevalier, C., Stojanović, O., Colin, D.J., Suarez-Zamorano, N., Tarallo, V., Veyrat-Durebex, C., Rigo, D.,
420 Fabbiano, S., Stevanović, A., Hagemann, S., et al. (2015). Gut Microbiota Orchestrates Energy
421 Homeostasis during Cold. Cell *163*, 1360–1374.

422 Cokelaer, T., Pultz, D., Harder, L.M., Serra-Musach, J., and Saez-Rodriguez, J. (2013). BioServices: a
423 common Python package to access biological Web Services programmatically. Bioinformatics *29*,
424 3241–3242.

425 Costea, P.I., Coelho, L.P., Sunagawa, S., Munch, R., Huerta-Cepas, J., Forslund, K., Hildebrand, F.,
426 Kushugulova, A., Zeller, G., and Bork, P. (2017). Subspecies in the global human gut microbiome. Mol.
427 Syst. Biol. *13*, 960.

428 Cypess, A.M., Weiner, L.S., Roberts-Toler, C., Elía, E.F., Kessler, S.H., Kahn, P.A., English, J., Chatman,
429 K., Trauger, S.A., Doria, A., et al. (2015). Activation of Human Brown Adipose Tissue by a β3-
430 Adrenergic Receptor Agonist. Cell Metab. *21*, 33–38.

431 Dheilly, N.M., Gänzle, M., Zheng, J., Chun, J., Park, S., Steinegger, M., and Cho, H.-S. (2020).
432 Metagenomic Association Analysis of Gut Symbiont Limosilactobacillus reuteri Without Host-Specific
433 Genome Isolation.

434 Fabbiano, S., Suárez-Zamorano, N., Chevalier, C., Lazarević, V., Kieser, S., Rigo, D., Leo, S., Veyrat-
435 Durebex, C., Gaïa, N., Maresca, M., et al. (2018). Functional Gut Microbiota Remodeling Contributes
436 to the Caloric Restriction-Induced Metabolic Improvements. Cell Metab. *0*.

437 Frese, S.A., Benson, A.K., Tannock, G.W., Loach, D.M., Kim, J., Zhang, M., Oh, P.L., Heng, N.C.K., Patil,
438 P.B., Juge, N., et al. (2011). The Evolution of Host Specialization in the Vertebrate Gut Symbiont
439 Lactobacillus reuteri. PLoS Genet. *7*, e1001314.

440 Garzetti, D., Brugiroux, S., Bunk, B., Pukall, R., McCoy, K.D., Macpherson, A.J., and Stecher, B. (2017).
441 High-Quality Whole-Genome Sequences of the Oligo-Mouse-Microbiota Bacterial Community.
442 Genome Announc. *5*, e00758-17.

443 Ghorbani, M., Claus, T.H., and Himms-Hagen, J. (1997). Hypertrophy of brown adipocytes in brown
444 and white adipose tissues and reversal of diet-induced obesity in rats treated with a β3-adrenoceptor
445 agonist. Biochem. Pharmacol. *54*, 121–131.

446 Guerra, C., Koza, R.A., Yamashita, H., Walsh, K., and Kozak, L.P. (1998). Emergence of brown
447 adipocytes in white fat in mice is under genetic control. Effects on body weight and adiposity. J. Clin.
448 Invest. *102*, 412–420.

449 Hugenholtz, F., and de Vos, W.M. (2018). Mouse models for human intestinal microbiota research: a
450 critical evaluation. Cell. Mol. Life Sci. *75*, 149–160.

451 Jain, C., Rodriguez-R, L.M., Phillippy, A.M., Konstantinidis, K.T., and Aluru, S. (2018). High throughput
452 ANI analysis of 90K prokaryotic genomes reveals clear species boundaries. Nat. Commun. *9*, 5114.

453 Johnson, J.S., Spakowicz, D.J., Hong, B.-Y., Petersen, L.M., Demkowicz, P., Chen, L., Leopold, S.R.,
454 Hanson, B.M., Agresta, H.O., Gerstein, M., et al. (2019). Evaluation of 16S rRNA gene sequencing for
455 species and strain-level microbiome analysis. Nat. Commun. *10*, 5029.

Kang, D., Li, F., Kirton, E.S., Thomas, A., Egan, R.S., An, H., and Wang, Z. (2019). MetaBAT 2: an adaptive binning algorithm for robust and efficient genome reconstruction from metagenome assemblies. 0–10.

Karlsson, F.H., Fåk, F., Nookaew, I., Tremaroli, V., Fagerberg, B., Petranovic, D., Bäckhed, F., and Nielsen, J. (2012). Symptomatic atherosclerosis is associated with an altered gut metagenome. Nat. Commun. *3*, 1245.

Kieser, S., Brown, J., Zdobnov, E.M., Trajkovski, M., and McCue, L.A. (2020). ATLAS: a Snakemake workflow for assembly, annotation, and genomic binning of metagenome sequence data. BMC Bioinformatics *21*, 257.

Kim, K.-H., Kim, Y.H., Son, J.E., Lee, J.H., Kim, S., Choe, M.S., Moon, J.H., Zhong, J., Fu, K., Lenglin, F., et al. (2017). Intermittent fasting promotes adipose thermogenesis and metabolic homeostasis via VEGF-mediated alternative activation of macrophage. Cell Res. *27*, 1309–1326.

Kopecky, J., Clarke, G., Enerbäck, S., Spiegelman, B., and Kozak, L.P. (1995). Expression of the mitochondrial uncoupling protein gene from the aP2 gene promoter prevents genetic obesity. J. Clin. Invest. *96*, 2914–2923.

Krych, L., Hansen, C.H.F., Hansen, A.K., van den Berg, F.W.J., and Nielsen, D.S. (2013). Quantitatively Different, yet Qualitatively Alike: A Meta-Analysis of the Mouse Core Gut Microbiome with a View towards the Human Gut Microbiome. PLoS One *8*, e62578.

Lagkouvardos, I., Pukall, R., Abt, B., Foesel, B.U., Meier-Kolthoff, J.P., Kumar, N., Bresciani, A., Martínez, I., Just, S., Ziegler, C., et al. (2016). The Mouse Intestinal Bacterial Collection (miBC) provides host-specific insight into cultured diversity and functional potential of the gut microbiota. Nat. Microbiol. *1*, 16131.

Lesker, T.R., Durairaj, A.C., Gálvez, E.J.C., Lagkouvardos, I., Baines, J.F., Clavel, T., Sczyrba, A., McHardy, A.C., and Strowig, T. (2020). An Integrated Metagenome Catalog Reveals New Insights into the Murine Gut Microbiome. Cell Rep. *30*, 2909-2922.e6.

Letunic, I., and Bork, P. (2019). Interactive Tree Of Life (iTOL) v4: recent updates and new developments. Nucleic Acids Res. *47*, W256–W259.

Li, G., Xie, C., Lu, S., Nichols, R.G., Tian, Y., Li, L., Patel, D., Ma, Y., Brocker, C.N., Yan, T., et al. (2017). Intermittent Fasting Promotes White Adipose Browning and Decreases Obesity by Shaping the Gut Microbiota. Cell Metab. *26*, 672-685.e4.

Liu, C., Zhou, N., Du, M.X., Sun, Y.T., Wang, K., Wang, Y.J., Li, D.H., Yu, H.Y., Song, Y., Bai, B.B., et al. (2020). The Mouse Gut Microbial Biobank expands the coverage of cultured bacteria. Nat. Commun. *11*.

Mills, E.L., Pierce, K.A., Jedrychowski, M.P., Garrity, R., Winther, S., Vidoni, S., Yoneshiro, T., Spinelli, J.B., Lu, G.Z., Kazak, L., et al. (2018). Accumulation of succinate controls activation of adipose tissue thermogenesis. Nature *560*, 102–106.

Nayfach, S., Shi, Z.J., Seshadri, R., Pollard, K.S., and Kyrpides, N. (2019). Novel insights from uncultivated genomes of the global human gut microbiome. Nature.

Nguyen, T.L.A., Vieira-Silva, S., Liston, A., and Raes, J. (2015). How informative is the mouse for human gut microbiota research? DMM Dis. Model. Mech. *8*, 1–16.

Nurk, S., Meleshko, D., Korobeynikov, A., and Pevzner, P.A. (2017). metaSPAdes: a new versatile metagenomic assembler. Genome Res. *27*, 824–834.

498 Okla, M., Wang, W., Kang, I., Pashaj, A., Carr, T., and Chung, S. (2015). Activation of Toll-like Receptor
499 4 (TLR4) Attenuates Adaptive Thermogenesis via Endoplasmic Reticulum Stress. J. Biol. Chem. *290*,
500 26476–26490.

501 Olm, M.R., Crits-Christoph, A., Diamond, S., Lavy, A., Carnevali, P.B.M., and Banfield, J.F. (2019).
502 Consistent metagenome-derived metrics verify and define bacterial species boundaries. BioRxiv
503 647511.

504 Parks, D.H., Imelfort, M., Skennerton, C.T., Hugenholtz, P., and Tyson, G.W. (2015). CheckM: assessing
505 the quality of microbial genomes recovered from isolates, single cells, and metagenomes. Genome
506 Res. *25*, 1043–1055.

507 Parks, D.H., Rinke, C., Chuvochina, M., Chaumeil, P.-A., Woodcroft, B.J., Evans, P.N., Hugenholtz, P.,
508 and Tyson, G.W. (2017). Recovery of nearly 8,000 metagenome-assembled genomes substantially
509 expands the tree of life. Nat. Microbiol. *2*, 1533–1542.

510 Parks, D.H., Chuvochina, M., Waite, D.W., Rinke, C., Skarshewski, A., Chaumeil, P.-A., and Hugenholtz,
511 P. (2018). A standardized bacterial taxonomy based on genome phylogeny substantially revises the
512 tree of life. Nat. Biotechnol. *36*, 996–1004.

513 Parks, D.H., Chuvochina, M., Chaumeil, P.-A., Rinke, C., Mussig, A.J., and Hugenholtz, P. (2020). A
514 complete domain-to-species taxonomy for Bacteria and Archaea. Nat. Biotechnol. 1–8.

515 Pasolli, E., Asnicar, F., Manara, S., Zolfo, M., Karcher, N., Armanini, F., Beghini, F., Manghi, P., Tett, A.,
516 Ghensi, P., et al. Extensive Unexplored Human Microbiome Diversity Revealed by Over 150,000
517 Genomes from Metagenomes Spanning Age, Geography, and Lifestyle. Cell *176*, 649-662.e20.

518 Price, M.N., Dehal, P.S., and Arkin, A.P. (2010). FastTree 2 - Approximately maximum-likelihood trees
519 for large alignments. PLoS One *5*, e9490.

520 Root, R.B. (1967). The Niche Exploitation Pattern of the Blue-Gray Gnatcatcher. Ecol. Monogr. *37*,
521 317–350.

522 Van Rossum, T., Ferretti, P., Maistrenko, O.M., and Bork, P. (2020). Diversity within species:
523 interpreting strains in microbiomes. Nat. Rev. Microbiol. *18*, 491–506.

524 Shaffer, M., Borton, M.A., McGivern, B.B., Zayed, A.A., La Rosa, S.L., Solden, L.M., Liu, P., Narrowe,
525 A.B., Rodríguez-Ramos, J., Bolduc, B., et al. (2020). DRAM for distilling microbial metabolism to
526 automate the curation of microbiome function. Nucleic Acids Res. *48*, 8883–8900.

527 Sieber, C.M.K., Probst, A.J., Sharrar, A., Thomas, B.C., Hess, M., Tringe, S.G., and Banfield, J.F. (2018).
528 Recovery of genomes from metagenomes via a dereplication, aggregation and scoring strategy. Nat.
529 Microbiol. *3*, 836–843.

530 Stewart, R.D., Auffret, M.D., Warr, A., Wiser, A.H., Press, M.O., Langford, K.W., Liachko, I., Snelling,
531 T.J., Dewhurst, R.J., Walker, A.W., et al. (2018). Assembly of 913 microbial genomes from
532 metagenomic sequencing of the cow rumen. Nat. Commun. *9*, 870.

533 Stojanović, O., Kieser, S., and Trajkovski, M. (2018). Common traits between the beige fat-inducing
534 stimuli. Curr. Opin. Cell Biol. *55*, 67–73.

535 Virtanen, P., Gommers, R., Oliphant, T.E., Haberland, M., Reddy, T., Cournapeau, D., Burovski, E.,
536 Peterson, P., Weckesser, W., Bright, J., et al. (2020). SciPy 1.0: fundamental algorithms for scientific
537 computing in Python. Nat. Methods *17*, 261–272.

538 Wood, D.E., Lu, J., and Langmead, B. (2019). Improved metagenomic analysis with Kraken 2. Genome

539 Biol. *20*, 257.

540 Wu, Y.-W., Simmons, B.A., and Singer, S.W. (2016). MaxBin 2.0: an automated binning algorithm to
541 recover genomes from multiple metagenomic datasets. Bioinformatics *32*, 605–607.

542 Xiao, L., Feng, Q., Liang, S., Sonne, S.B., Xia, Z., Qiu, X., Li, X., Long, H., Zhang, J., Zhang, D., et al.
543 (2015). A catalog of the mouse gut metagenome. Nat. Biotechnol. *33*, 1103–1108.

544 Zhao, X. (2018). BinDash, software for fast genome distance estimation on a typical personal laptop.
545 Bioinformatics.

546 Ziętak, M., Kovatcheva-Datchary, P., Markiewicz, L.H., Ståhlman, M., Kozak, L.P., and Bäckhed, F.
547 (2016). Altered Microbiota Contributes to Reduced Diet-Induced Obesity upon Cold Exposure. Cell
548 Metab. *23*, 1216–1223.

549